Combustion and Flame 288 (2026) 114966

Contents lists available at ScienceDirect

Combustion and Flame

journal homepage: www.sciencedirect.com/journal/combustion-and-flame

# Flow reactor study of $NH_3$/DMM oxidation

Adrián Ruiz-Gutiérrez, Daniel Mazano-Peña, María U. Alzueta *

*Aragón Institute of Engineering Research (I3A), Department of Chemical and Environmental Engineering, University of Zaragoza, 50018, Zaragoza, Spain*

ARTICLE INFO

*Keywords:*
$NH_3$
DMM
Kinetic modelling
Co-firing
Flow reactor

ABSTRACT

This study presents a comprehensive investigation of the conversion of ammonia ($NH_3$) and dimethoxymethane (DMM) mixtures in a quartz flow reactor. Experiments were carried out at atmospheric pressure and across a wide range of conditions to elucidate species profiles, many of which have not been extensively characterised previously. The operational parameters included temperatures between 875 and 1425 K, $NH_3$/DMM ratios from 0.48 to 10.86, and oxygen excess ratios (λ) from 0 to 3.12. Quantification of numerous compounds was achieved using a micro gas chromatograph (GC) in combination with a continuous gas analyser. Simulations with an updated detailed chemical kinetic mechanism were carried out in order to elucidate the conversion pathways of the mixture constituents. Calculations were in good consistency with the experimentally observed ones for the key species. $NH_3$ conversion was highly sensitive to variations in $O_2$, whereas DMM exhibited only minor changes in its reaction temperature (approximately 50 K). The principal consumption pathway of DMM involves hydrogen abstraction from the central carbon by $CH_3$ radicals. This facilitates the access of ammonia to a greater number of radicals, as competition for OH or O radicals is less pronounced. NO formation was influenced by the presence of DMM, increasing with both the oxygen excess ratio (λ) and the proportion of DMM in the mixture. It was further concluded that DMM exerts a significant influence on $NH_3$ behaviour when the $NH_3$/DMM ratio is $\leq$ 1, an effect that decreases at higher initial $O_2$ concentrations ($\lambda > 1$). Overall, this work provides new insights into the conversion behaviour of $NH_3$/DMM mixtures under the investigated conditions and provides essential reference data for further development of detailed kinetic models.

## 1. Introduction

At current levels of energy consumption, there remains a significant reliance on conventional fossil fuels, primarily due to their high energy density and versatility. However, these fuels have been shown to contribute substantially to greenhouse gas emissions, notably $CO_2$ and $CH_4$. In 2022, within the European Union (EU), the electricity supply and transport sectors were the principal sources of such emissions, accounting for 27.4% and 23.8% respectively [1]. Energy production across the EU continues to rely predominantly on conventional fuels, with certain member states generating most of their electricity from fossil sources [2].

Emissions are gradually declining, driven by the expanding use of renewable energy sources, particularly within the electricity generation sector, which achieved a 16.5% reduction in emissions across the European Union (EU) [3]. Notably, countries such as Portugal and Austria now generate over 70% of their electricity from renewable sources. However, electricity consumption constitutes only a fraction of total energy use. Therefore, the development of more environmentally sustainable fuels will be essential for future energy applications. In this context, the investigation of alternative fuels becomes particularly relevant. These can be produced through the 'Power-to-Fuel' approach, whereby surplus renewable energy is used to synthesize fuels.

One of the fuels that could be developed under this strategy is ammonia ($NH_3$). Its appeal lies in the fact that both its synthesis and storage technologies are already well established, making it one of the most widely synthesized chemical compounds globally [4]. Moreover, it has been demonstrated that 'green ammonia' can be produced using energy derived from renewable sources [5].

Although ammonia is an excellent hydrogen storage medium, it has a relatively high energy density and is a carbon-free fuel, its combustion presents several key disadvantages, such as a high ignition temperature, significantly lower energy density than conventional fuels, and the formation of nitrogen oxides ($NO_x$).

To overcome these disadvantages, the most widely adopted approach is co-firing ammonia with other fuels that exhibit more

* Corresponding author.
*E-mail address:* uxue@unizar.es (M.U. Alzueta).

https://doi.org/10.1016/j.combustflame.2026.114966
Received 16 January 2026; Received in revised form 23 March 2026; Accepted 23 March 2026
Available online 28 March 2026

favorable thermochemical properties. Research involving oxygenated compounds, particularly methanol ($CH_3OH$), dimethyl ether (DME), and diethyl ether (DEE), has demonstrated significant improvements compared to net ammonia. Notable changes have been observed in key combustion parameters, including reduced ignition delay times (IDTs) [6–8], improved ammonia conversion [9,10], and increased laminar burning velocities (LBVs) [6,11,12]. Oxygenated methyl groups (OMEx) are gaining increasing relevance due to their high cetane number, elevated $O_2$ content, and absence of C—C bonds, which typically inhibit ash formation [13,14]. Considering these factors, the investigation of the simplest OME, dimethoxymethane (DMM), is of particular interest. DMM contains 42% (w/w) oxygen [15], exhibits greater solubility in diesel than other ethers, such as DEE, possesses a higher cetane number, and has a lower vapor pressure [16]. Additionally, this compound can potentially be synthesized from $CH_3OH$ [17].

DMM has been tested in blends with diesel, demonstrating reductions in emissions, improved engine performance, and lower ash formation [18]. The reduction in ash is attributed to the generation of fewer intermediate species that serve as precursors to soot in the ambient air [19]. Additionally, the addition of DMM has been shown to decrease $NO_x$ emissions [16].

Experimental investigations into this fuel mixture remain limited, with the predominant methodologies being the constant-volume spherical vessel (CVSV) [20], the shock tube [21], and the constant-volume combustion chamber [22]. The laminar burning velocity, another critical parameter, increases significantly when DMM is added to $NH_3$ mixtures in comparison with mixtures such as $NH_3/CH_4$ [20]; in some cases, increases of up to threefold have been reported. Ignition delay times (IDT) of $NH_3$/DMM mixtures have also been studied, with notable reductions observed relative to pure $NH_3$. This improvement becomes more significant as the proportion of DMM in the mixture increases [20], likely due to the generation of additional reactive radicals from DMM enrichment, which accelerate the chain-reaction mechanisms in which $NH_3$ is involved [23].

Owing to the promising performance of $NH_3$/DMM fuel mixtures, further research is required to elucidate their conversion pathways. Although only a limited number of studies exist, detailed species profiles during oxidation remain virtually unexplored. This work therefore investigates $NH_3$/DMM conversion through both experiments and kinetic modelling across a wider range of conditions than previously reported, including 875–1425 K, $NH_3$/DMM ratios from 0.45 to 10.86, and oxygen excess ratios (λ) between 0 and 3.12. The results provide new insights into species behavior under these conditions and supply baseline data to support the development of detailed kinetic models.

## 2. Experimental

The experiments were conducted in a quartz flow reactor with an internal diameter of 8.7 mm and a reaction length of 200 mm. The reactor has four inlets, three at the top, through which the reagents diluted in argon are added, and one on the side, used for the carrier gas, in this case argon. In this way, it was possible to work in an inert atmosphere. A detailed diagram of the setup and a figure showing the flow reactor are presented in Fig. S1-S2 of the Supplementary Material. The primary argon stream was preheated before mixing with the reactive components. Reactants are only mixed in the reaction zone. Gas flows were regulated using Alicat mass flow controllers. A gas flow rate of 1 $L{\cdot}min^{-1}$ (STP) was used in all experiments. Concerning residence time ($t_r$), at 1000 K, this corresponds to a $t_r$ of approximately 190 ms, calculated based on the specific temperature and pressure conditions. The experimental setup is based on that described by Alzueta et al. (2001) [24], which has been successfully used in previous works investigating various organic oxygenated compounds blended with ammonia [9,10,16].

The reactor is placed inside an electric oven to maintain isothermal conditions. A temperature profile was created with a precision of ±5 K, verified using a type-K thermocouple. The temperature profile along the 200 mm reactor length is shown in Fig. S3 of the Supplementary Material.

**Table 1**
Experimental conditions. Balance is closed with Ar. Concentrations are expressed in ppm. Set 11 is from [25]. Concentrations are given in ppm.

| Set | $NH_3$ | DMM | $NH_3$/DMM | λ | $t_r$ (s) |
|---|---|---|---|---|---|
| 1 | 997 | 982 | 1.02 | 0 | 190/T(K) |
| 2 | 1024 | 999 | 1.03 | 0.48 | 190/T(K) |
| 3 | 997 | 996 | 1.00 | 0.98 | 192/T(K) |
| 3R | 1011 | 1004 | 1.01 | 1.00 | 190/T(K) |
| 4 | 976 | 976 | 1.00 | 3.12 | 191/T(K) |
| 5 | 474 | 1004 | 0.47 | 0.50 | 191/T(K) |
| 6 | 490 | 1038 | 0.47 | 0.93 | 189/T(K) |
| 7 | 454 | 948 | 0.48 | 3.2 | 191/T(K) |
| 8 | 1029 | 95 | 10.83 | 0.49 | 190/T(K) |
| 9 | 987 | 98 | 10.07 | 1.03 | 190/T(K) |
| 10 | 997 | 95 | 10.49 | 3.03 | 191/T(K) |
| 11 | 0 | 653 | 0.00 | 1.00 | 195/T(K) |

An Agilent 990 Micro GC gas chromatograph equipped with TCD detectors was used to quantify the majority of the compounds (DMM, $CH_3OH$, CO, $CO_2$, $CH_4$, $C_2H_6$, $C_2H_4$, $C_2H_2$, $NH_3$, $N_2O$, $N_2$, $H_2$, $O_2$, and HCN). The standard deviation of measurements is consistent across the temperature range considered for certified reference gasses, with a maximum error of ±10 ppm. A continuous gas analyzer (Advance Optima AO2020) was employed to detect and quantify NO, with a 1% uncertainty and a minimum detection threshold of 10 ppm. $NO_2$ concentration was checked with a continuous analyzer of the same company, and was found to be negligible for all experimental conditions.

Experiments were conducted systematically varying temperature, oxygen excess ratio (λ), and fuel mixture ratio. The complete experimental set is summarized in Table 1. λ is defined as the ratio of the oxygen concentration present in the reaction zone and the stoichiometric oxygen demand, as determined from the overall balanced chemical reactions to produce $N_2$ and $CO_2$ from ammonia and DMM, respectively.

$$NH_3 + 0.75O_2 \rightarrow 0.5N_2 + 1.5H_2O \quad (1)$$

$$DMM + 4O_2 \rightarrow 3CO_2 + 4H_2O \quad (2)$$

Set 1 in Table 1 corresponds to pyrolysis conditions. The combined effects of oxygen concentration and $NH_3$/DMM mixture ratio were studied. Sets 1–4 illustrate the influence of oxygen at constant $NH_3$ and DMM concentrations. Sets 3 and 3R are repeated experiments to demonstrate reproducibility. Finally, additional experiments with λ from 0.48 to 3.20 and $NH_3$/DMM ratios from 0.48 to 10.86 are reported as sets 5–10.

A mass balance for carbon and nitrogen was carried out for each experiment, using both experimental and calculated results. No

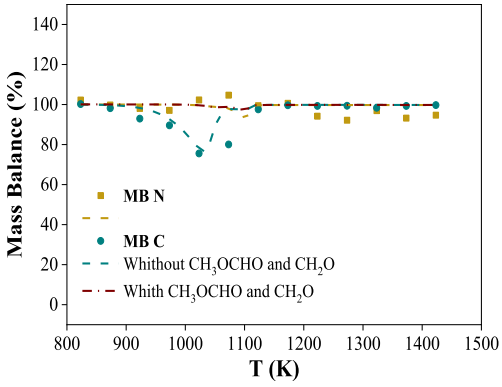


**Fig. 1.** Carbon and nitrogen mass balance for Set 3.

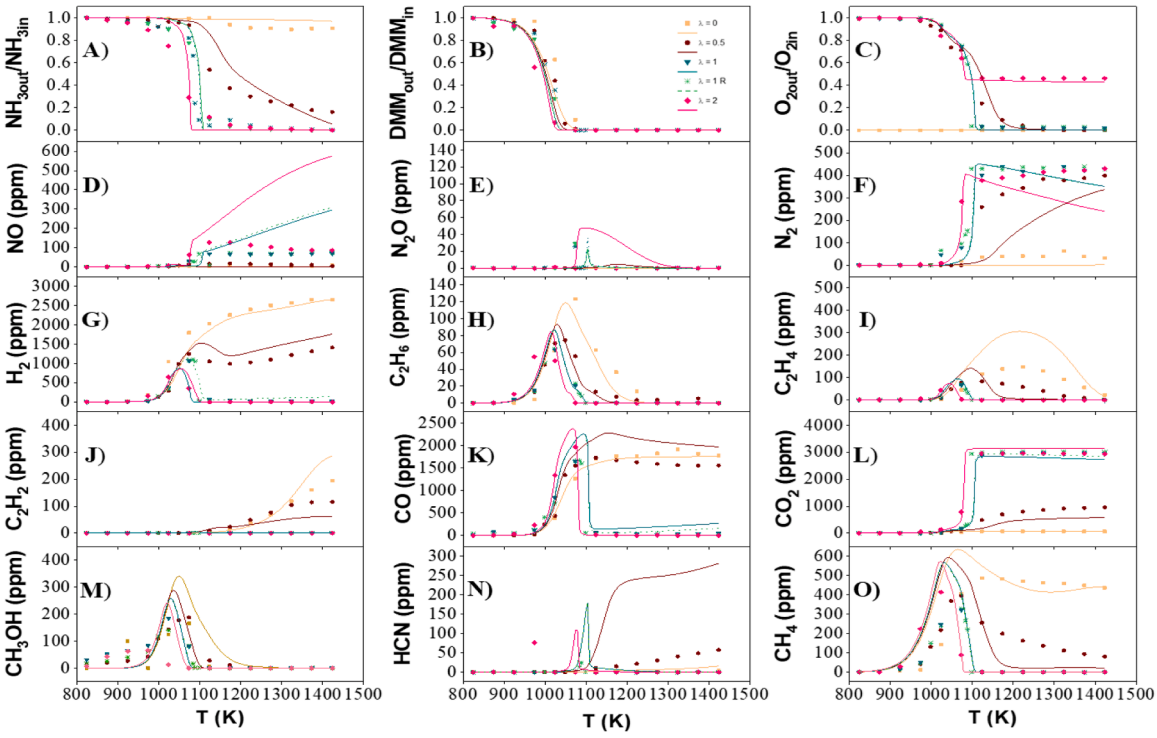


**Fig. 2.** Concentrations of the most important product species for $NH_3$/DMM = 1 for different λ (Sets 1, 3–5 of Table 1). $NH_3$, DMM and $O_2$, as reactants, are shown as normalised values.

significant discrepancies were observed in the nitrogen mass balance, with errors consistently below 10%, which are mainly attributed to the lack of identification of some species in low concentrations in the analysis. However, the same behaviour was not observed for carbon, as a reduction in the amount of carbon accounted for was noted in the 950–1075 K temperature range, both in experiments and calculations. Within this temperature range, the kinetic model predicts the formation of methyl formate ($CH_3OCHO$) and formaldehyde ($CH_2O$) which were not measured during experiments. Including these compounds in the carbon calculated balance mitigates the observed decrease in carbon, which is an indication that the rest of the species are well captured in the experiments. Fig. 1 illustrates this for one representative example (Set 3). The rest mass balances are provided in Fig. S4 of the Supplementary Material.

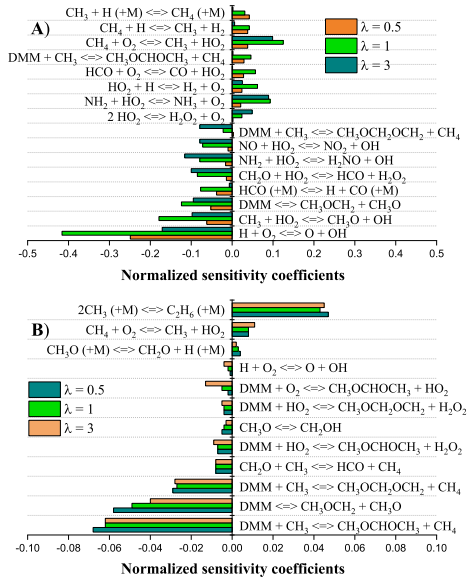


**Fig. 3.** Sensitivity analysis for (A) $NH_3$ and (B) DMM at 10% conversion for different λ. In ascending order of λ. Sets 2–4 in Table 1.

## 3. Kinetic modelling

The mechanism employed is derived from that reported in a previous study of the $NH_3$/DEE fuel mixture [26]. It incorporates the nitrogen chemistry by Glarborg et al. [27], with a series of updates for $NH_3$, $CH_3CN$ and $NH_3$-NO [28]. In addition, some important reactions in ammonia chemistry have been updated in the present work, such as $NH_2 + HO_2 \rightleftharpoons H_2NO + OH$ (r3), $NH_2 + HNO \rightleftharpoons NH_3 + NO$ (r4), and $HNO + H (+M) \rightleftharpoons H_2NO (+M)$ (r5), which are found to enhance the overall conversion of nitrogen compounds, based on the work presented by Jian et al. [29]. Other reactions involving HNCO, NCO, and $CH_3NH_2$ were revised as proposed by Morell et al. [30]. With respect to carbon chemistry, the mechanism includes reaction subsets of different oxygenated compounds [9,10,26], with the main oxidation chemistry of DME and DEE adopted from the work of Marrodán et al. [31] and Tran et al. [32], respectively. The initial sub-mechanism for DMM oxidation is based on the work of Marrodán et al. [33], dealing with high-pressure $C_2H_2$-DMM mixtures.

Some of the subsequent additions correspond to those proposed by García-Ruiz et al. [34], based on the N—C interactions between $CH_3O$-$CH_2O$, $CH_3O$, $CH_2OH$ and HCO with NO and $NH_2$. All these reactions were taken from the work of Dai et al. [21]. Other notable modifications concern those introduced for C—N interactions [35,36], as they provide a better agreement between the calculated results and the experimental data. Concerning the most notable modifications in the DMM oxidation subset, the thermal decomposition reactions of DMM, DMM $\rightleftharpoons CH_3OCH_2 + CH_3O$ (r6) and DMM $\rightleftharpoons CH_3OCH_2O + CH_3$ (r7), proposed by Sun et al. [37], interactions between DMM and nitrogen species [38], $NH_2$–DMM [39], and $NH_2$–$CH_3OCH_2OCH_2$ [21], were added.

## 4. Results and discussions

### 4.1. Influence of the oxygen excess ratio

Sets 1–4 in Table 1 are selected to study the influence of oxygen on fuel oxidation. The species profiles of all measured compounds are presented in Fig. 2.

Fig. 2A shows the species profile for $NH_3$ over the temperature range 875–1425 K for different values of λ. The increase in λ causes a shift to lower temperatures in $NH_3$ consumption. There is a difference of approximately 100 K in the onset of the fuel-rich to fuel-lean transition. $NH_3$ is completely consumed for $\lambda \geq 1$, whereas under fuel-rich conditions, 16% of the fuel remains unoxidized under the studied conditions. Calculations agree reasonably well with the experimental results.

The primary reactions responsible for ammonia consumption involve its interaction with OH and O radicals, $NH_3 + OH \rightleftharpoons NH_2 + H_2O$ (r8) and $NH_3 + O \rightleftharpoons NH_2 + OH$ (r9), respectively. This behavior is similar to that happening with other ethers such as DEE [24]. However, the interactions of $NH_2$ radical with hydrogen can recycle back $NH_3$ under all conditions, $NH_2 + H_2 \rightleftharpoons NH_3 + H$ (r10). Additionally, the radical $HO_2$ also causes recycling back ammonia through the reaction $NH_2 + HO_2 \rightleftharpoons NH_3 + O_2$ (r11) under fuel-lean conditions.

Fig. 3A shows the sensitivity analysis of $NH_3$ at the temperature corresponding to 10% consumption. Reactions that promote a higher concentration of OH radicals, such as $H + O_2 \rightleftharpoons O + OH$ (r12) or $CH_3 + HO_2 \rightleftharpoons CH_3O + OH$ (r13), play a significant role in ammonia consumption. Results are more sensitive under stoichiometric conditions. The increase in $O_2$ also favors more reactions involving the $HO_2$ radical, such as $CH_2O + HO_2 \rightleftharpoons HCO + H_2O_2$ (r14). This further promotes $NH_3$ consumption through the decomposition of $H_2O_2$, $H_2O_2$ (+M) $\rightleftharpoons$ 2OH (+M) (r15). Simultaneously, the thermal decomposition of DMM, DMM $\rightleftharpoons CH_3OCH_2 + CH_3O$ (r6), and the consumption of DMM by secondary pathways, e.g. DMM + $CH_3 \rightleftharpoons CH_3OCH_2OCH_2 + CH_4$ (r16), not involving the O/H radical pool, promote the consumption of $NH_3$.

Regarding the inhibition of $NH_3$ consumption, $HO_2$ formation is one of the main limiting factors, occurring via the reaction $CH_4 + O_2 \rightleftharpoons CH_3 + HO_2$ (r17). It is also illustrated in Fig. 3A, where half of the most inhibitory reactions are associated with $CH_4$ formation pathways, such as DMM + $CH_3 \rightleftharpoons CH_3OCHOCH_3 + CH_4$ (r18). $HO_2$ plays a key role in inhibiting $NH_3$ consumption, with reactions such as $NH_2 + HO_2 \rightleftharpoons NH_3 + OH$ (r19).

The nitrogen compounds produced from the oxidation of $NH_3$ are $N_2$, NO, $N_2O$ and HCN. Nitrous oxide (Fig. 2E) has only been detected in appreciable quantities under stoichiometric conditions, at levels above 30 ppm. This is consistent with the kinetic model estimations. However, the calculations indicate an increase in $N_2O$ concentration in both fuel-rich and fuel-lean conditions, which has not been identified experimentally, this requires further research in the future.

NO is one of the most abundant undesired emissions resulting from the oxidation of $NH_3$. Fig. 2D shows the rise in NO formation with increasing $O_2$ availability in the reactor. Although the overall behavior is captured by the calculations, at high temperatures the kinetic model overestimates NO production. Under fuel-rich conditions, NO production is mainly caused by $C_2H_4 + HNO \rightleftharpoons C_2H_5 + NO$ (-r20) and $CH_3ONO$ (+M) $\rightleftharpoons CH_3O + NO$ (+M) (-r21). At higher initial λ, only reaction (–r21) contributes significantly, as it derives from $CH_3 + NO_2 \rightleftharpoons CH_3ONO$ (–r22).

For NO consumption, the main reactions are $NH_2 + NO \rightleftharpoons N_2 + H_2O$ (r23), $NH_2 + NO \rightleftharpoons NNH + OH$ (r24), and $NO + HO_2 \rightleftharpoons NO_2 + OH$ (r25). The (r23) and (r24) reactions are more relevant when $\lambda \leq 1$, while (r24) is predominant for fuel-lean conditions, due to the pronounced increase in $HO_2$ radical in the reaction zone. However, reaction (r24) is not significant to show appreciable amounts of $NO_2$ in the exhaust gas.

The sensitivity analysis of NO at a concentration of 10 ppm is consistent with the preceding results, since reactions that produce more radicals $CH_3$ or $HO_2$, $CH_4$ (+M) $\rightleftharpoons CH_3 + H$ (+M) (-r26) and $H + O_2$ (+M) $\rightleftharpoons HO_2$ (+M) (r27), promote NO consumption.

On the contrary, the production of OH radicals by pathways such as $H + O_2 \rightleftharpoons O + OH$ (r12) and $NH + O \rightleftharpoons NO + OH$ (r28) inhibits NO consumption, due to the enhancement of $NH_2$ radicals resulting from the higher concentration of OH radicals. The consumption of $CH_3$ radicals by pathways other than (-r22) also significantly inhibits NO production. This trend can be observed in the sensitivity analysis presented in Fig. S5 of the Supplementary Material.

Regarding $N_2$ (Fig. 2F), the main nitrogen product of ammonia conversion under the studied conditions, the increase in temperature leads to a peak in its production, driven by intensified $NH_3$ consumption. A difference of 150 K is observed between the onset of $N_2$ production under fuel-rich and fuel-lean conditions. The main $N_2$-producing reactions are interaction with the formed NO, $NH_2 + NO \rightleftharpoons N_2 + H_2O$ (r23), and direct oxidation: $NNH \rightleftharpoons N_2 + H$ (r29). Reaction (r22) is predominant under the conditions studied, gaining greater importance as the initial $O_2$ concentration increases.

HCN is a harmful toxic compound (Fig. 2N), and the peak concentration observed has been 76 ppm under fuel-lean conditions. However, in the presence of sufficient $O_2$, the temperature window in which this secondary product is formed is very narrow. HCN originates through $H_2CN \rightleftharpoons HCN + H$ (r30), with $H_2CN$ basically produced in reaction $CH_3 + NH_2 \rightleftharpoons CH_3NH_2$ (r31). HCN production shifts to higher temperatures as the concentration of $O_2$ in the medium is reduced. This is because important reactions in the consumption of HCN, such as $HCN + OH \rightleftharpoons CN + H_2O$ (r32) and $HCN + OH \rightleftharpoons HOCN + H$ (r33), are not relevant due to the low concentration of OH radicals. Calculated HCN is overestimated under fuel-rich conditions because $CH_3NH_2$ reacts predominantly via hydrogen abstraction channels, with no other radicals involved. As a result, the model overpredicts HCN in low $O_2$ concentration conditions. These observations highlight the need for further investigation of the decomposition pathway of $CH_3NH_2$, as well as potential interactions with the most abundant radicals in these conditions, such as $NH_2$ or $CH_3$. Previous works [e.g. 40] have already indicated the complex chemistry and interactions of $CH_3NH_2$ in the presence of $CH_4$.

As shown in Fig. 2G, $H_2$ exhibits different behavior depending on λ. In addition, the oxygen excess ratio also determines the temperature range over which significant concentrations of $H_2$ are observed at the reactor outlet. The initial increase in $H_2$ occurs through the same reaction mechanisms under the conditions studied, with the hydrogen abstraction from DMM when interacting with H radicals, DMM + $H \rightleftharpoons CH_3OCHOCH_3 + H_2$ (r34) and DMM + $H \rightleftharpoons CH_3OCH_2OCH_2 + H_2$ (r35). The only $H_2$ consumption channel at low temperatures is $CH_3 + H_2 \rightleftharpoons CH_4 + H$ (-r36).

Under pyrolysis conditions, the concentration of $H_2$ increases throughout the experiment because radicals are insufficient to consume it. Under fuel-rich conditions, $H_2$ concentration decreases slightly in the range of 1108–1178 K. This is because of the significant concentration of OH radicals, which participate in the reaction $OH + H_2 \rightleftharpoons H + H_2O$ (r37) at these temperatures. Subsequently, as most of the OH radicals are exhausted, (r37) loses weight, and the concentration of $H_2$ increases again. At high temperatures, $H_2$ does not come from the hydrogen abstraction of DMM, but from the consumption of $CH_4$, $CH_4 + H \rightleftharpoons CH_3 + H_2$ (r38), and $NH_2$ radicals, $NH_2 + H \rightleftharpoons NH + H_2$ (r39). For $\lambda \geq 1$, $H_2$ is produced from (r34) and (r35), being consumed mainly in the temperature range 1075–1125 K. The model predicts incomplete combustion of $H_2$ under stoichiometric conditions, although experimentally, no more than 16 ppm has been quantified at high temperatures.

DMM (Fig. 2B) reacts within a significantly narrower temperature interval than $NH_3$, namely between 925 and 1100 K. While an increase in λ promotes a slight acceleration in DMM consumption, the effect remains marginal, as the total consumption under the most unfavorable conditions differs by only 50 K.

In contrast to $NH_3$, DMM exhibits a markedly narrower temperature window for reaction than the other fuels studied, with the entire reaction process occurring between 875 and 1225 K. Under the most extreme

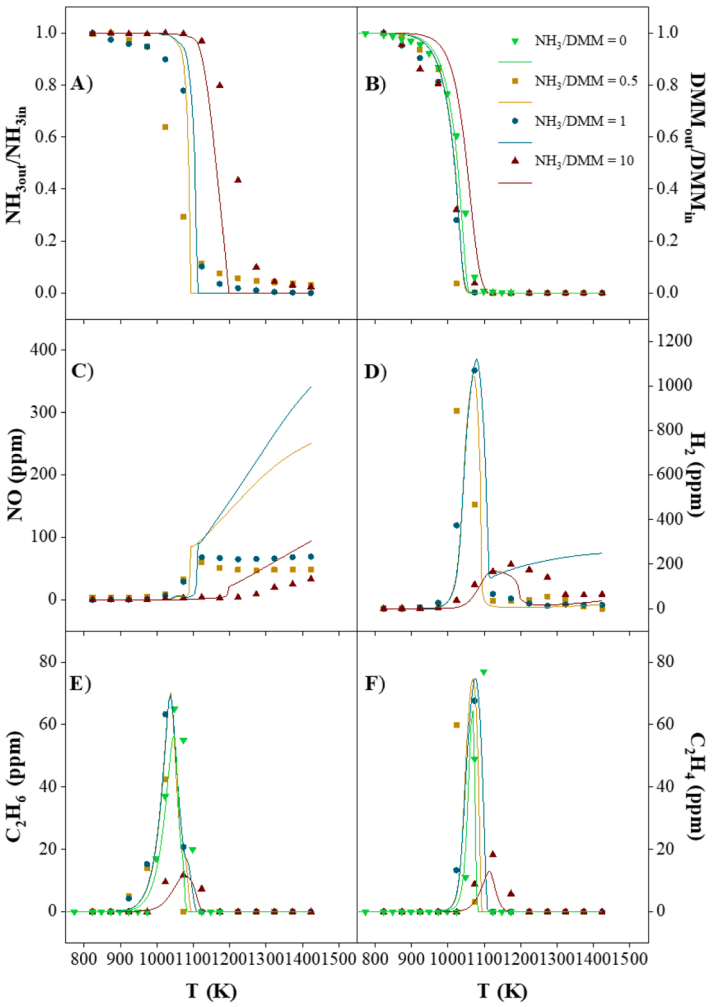


**Fig. 4.** Profile of species at $\lambda = 1$ for different $NH_3$/DMM ratios (Sets 3, 6, 9, and 11 of Table 1).

conditions, the temperature difference at which complete fuel consumption takes place is approximately 100 K. This behavior suggests that DMM is more strongly influenced by the initial $O_2$ concentration than fuels such as DEE [26].

Under pyrolysis conditions, calculations indicate that DMM consumption occurs primarily through its thermal decomposition, DMM ⇌ $CH_3OCH_2$ + $CH_3$ (r7). However, when $O_2$ is added to the mixture, this reaction pathway is altered, with interactions involving $CH_3$ radicals becoming significantly more important, such as DMM + $CH_3$ ⇌ $CH_3O$-$CHOCH_3$ + $CH_4$ (r16) and DMM + $CH_3$ ⇌ $CH_3OCH_2OCH_2$ + $CH_4$ (r16). The hydrogen abstraction from DMM by $CH_3$ radicals is the dominant pathway, with abstraction from the central carbon being preferred. As λ increases, the hydrogen abstraction through interactions with OH radicals becomes more relevant, e.g., DMM + OH ⇌ $CH_3OCHOCH_3$ + $H_2O$ (r40) and DMM + OH ⇌ $CH_3OCH_2OCH_2$ + $H_2O$ (41), although it never becomes the most significant pathway in any case.

To identify the reactions that significantly influence DMM consumption, a sensitivity analysis was performed (Fig. 3B), using the temperature at which 10% of the DMM had been consumed. It is observed that the hydrogen abstraction by $CH_3$ radicals plays a key role in DMM consumption, although its significance decreases as λ increases. This is due to the rise of other radicals that contribute to DMM consumption. Consequently, reactions such as DMM + $O_2$ ⇌ $CH_3OCHOCH_3$ + $HO_2$ (r42) and DMM + $HO_2$ ⇌ $CH_3OCHOCH_3$ + $H_2O_2$ (r43) become more important at higher λ values. Conversely, reactions that reduce the availability of $CH_3$ radicals, such as $2CH_3$ (+M) ⇌ $C_2H_6$ (+M) (r44), and reactions that generate $CH_3$ more slowly, such as $CH_4$ + $O_2$ ⇌ $CH_3$ + $HO_2$ (r17), are those that most inhibit DMM consumption. Ammonia does not appear to inhibit or enhance DMM consumption under the conditions studied, unlike other fuels in mixtures with $NH_3$ [10,25]. This is because DMM consumption is driven primarily by $CH_3$ radicals, rather than by other radicals that are more relevant in $NH_3$ consumption, like OH or O.

Methanol (Fig. 2M) is one of the most important intermediate compounds formed during DMM oxidation. In the experiments conducted, it is observed that higher $O_2$ concentrations result in lower $CH_3OH$ concentrations, whereas higher peaks are observed under the other conditions. However, under fuel-rich conditions, methanol appears at higher temperatures, indicating a shift in the temperature at which its maximum concentrations are reached. In the literature, the difficulties addressing $CH_3OH$ and $CH_2O$ detection have been mentioned [31,33]. However, the fact that calculations and experimental results coincide well, support the fact that we are in fact detecting methanol in the present experiments. The methanol formed originates predominantly from the thermal decomposition of methyl formate, $CH_3OCHO$ (+M) ⇌ $CH_3OH$ + CO (+M) (r45). At the same time, the consumption pathways of $CH_3OH$ are consistent across all λ values, with $CH_3OH$ + $CH_3$ ⇌ $CH_3O$ + $CH_4$ (r46) and $NH_2$ + $CH_3OH$ ⇌ $NH_3$ + $CH_2OH$ (r47) being the reactions responsible for the majority of $CH_3OH$ consumption. Interaction with $NH_2$ radicals is significant in $CH_3OH/NH_3$ mixtures, as indicated by previous studies [10,40].

Another important intermediate carbon compound in DMM oxidation is $CH_4$ (Fig. 2O). Similar to $CH_3OH$, the temperature at which its maximum concentration occurs shifts depending on the $O_2$ excess ratio.

As λ decreases, the $CH_4$ formation shifts toward higher temperatures. Under λ = 0.5, complete $CH_4$ consumption does not occur, with 8% of the initially introduced carbon remaining at high temperatures as methane. This is due to the lack of OH radicals, as $CH_4 + OH \rightleftharpoons CH_3 + H_2O$ (r48) is the dominant reaction for $CH_4$ consumption (λ > 0). Under pyrolysis conditions, the behavior differs, with $CH_4$ concentrations stabilizing at higher temperatures (T > 1125 K). This occurs in the calculations, which show $CH_4$ decreasing to 453 ppm. The model predicts that when DMM oxidizes rapidly at high temperatures, alternative $CH_4$ formation pathways, such as $CH_3 + H_2 \rightleftharpoons CH_4 + H$ (-r49) or $CH_3 + H (+M) \rightleftharpoons CH_4 (+M)$ (r50), do not produce the same amount of $CH_4$ as at lower temperatures.

Other products of DMM oxidation include $C_2H_6$ (Fig. 2H) and $C_2H_4$ (Fig. 2I). For a given temperature, the concentrations of these compounds increase as λ decreases. Furthermore, their presence persists over higher temperature ranges when $O_2$ concentrations in the reactor are lower. The pathway for ethane formation is consistent across all λ values studied, with ethane produced via $2CH_3 (+M) \rightleftharpoons C_2H_6 (+M)$ (r44). The consumption of $C_2H_6$ is indirectly linked to $C_2H_4$ formation through reactions such as $C_2H_6 + CH_3 \rightleftharpoons C_2H_5 + CH_4$ (r51), $C_2H_6 + H \rightleftharpoons C_2H_5 + H_2$ (r52), and $C_2H_6 + OH \rightleftharpoons C_2H_5 + H_2O$ (r53). These reactions generate $C_2H_5$, which serves as the primary intermediate for the formation of $C_2H_4$ via $C_2H_5 (+M) \rightleftharpoons C_2H_4 + H (+M)$ (r54).

Under pyrolysis conditions, $C_2H_4$ is consumed through interactions with $CH_3$ radicals, $C_2H_4 + CH_3 \rightleftharpoons C_3H_6 + H$ (r55) and $C_2H_4 + CH_3 \rightleftharpoons C_2H_3 + CH_4$ (r56), or with $NH_2$ radicals, $C_2H_4 + NH_2 \rightleftharpoons C_2H_3 + NH_3$ (r57). However, when $O_2$ is initially present, ethylene consumption occurs mainly through reactions with HNO and OH radicals, specifically $C_2H_4 + HNO \rightleftharpoons C_2H_3 + NO$ (r58) and $C_2H_4 + OH \rightleftharpoons C_2H_3 + H_2O$ (r59). The formation of $C_2H_3$ under fuel-rich conditions accounts for the subsequent formation of $C_2H_2$ via $C_2H_3 (+M) \rightleftharpoons C_2H_2 + H (+M)$ (r60). This compound is observed only at λ ≤ 0.5, with its concentration increasing at high temperatures.

CO (Fig. 2K) and $CO_2$ (Fig. 2L) are the main compounds in emissions from the combustion of carbon compounds. They exhibit behavior consistent with previous studies on carbon containing fuel mixtures [10, 26], although it varies with the initial $O_2$ concentration. At the start of CO generation, in the absence of $O_2$, formation of CO in small amounts occurs through $HNCO + H \rightleftharpoons CO + NH_2$ (r61) and $CH_2CO (+M) \rightleftharpoons CH_2 + CO (+M)$ (-r62), while in the presence of $O_2$, CO comes from the decomposition of $CH_3OCHO$, $CH_3OCHO (+M) \rightleftharpoons CH_3OH + CO (+M)$ (r45), and the consumption of HCO, $HCO (+M) \rightleftharpoons H + CO (+M)$ (r63) and $HCO + O_2 \rightleftharpoons CO + HO_2$ (r64). CO consumption coincides with $CO_2$ production, with the most important reactions being $CO + OH \rightleftharpoons CO_2 + H$ (r65) and $CO + HO_2 \rightleftharpoons CO_2 + OH$ (r66). This explains why, in fuel-rich conditions, CO is not consumed at high temperatures owing to the limited availability of OH and $HO_2$ radicals.

### 4.2. Influence of the $NH_3$/DMM ratio

Fig. 4 shows the species profiles of the compounds that exhibit a major change in their main production/consumption reactions when the $NH_3$/DMM ratio is changed. The remaining species profiles, as well as those obtained for another oxygen excess ratio conditions, are provided in Supplementary Material, Fig. S6–S8.

Regarding nitrogen compounds, variations were observed in the consumption of ammonia and nitrogen monoxide. A reduction in DMM concentration results in a shift of the main reaction zone by approximately 150 K (Fig. 4A) for $NH_3$. The key $NH_3$ consumption reactions are $NH_3 + OH \rightleftharpoons NH_2 + H_2O$ (r8) and $NH_3 + O \rightleftharpoons NH_2 + OH$ (r9). Pathways such as $NH_2 + HO_2 \rightleftharpoons NH_3 + O_2$ (r11) become less relevant under highly diluted DMM conditions. However, this does not compensate for the marked depletion of radical species. For $NH_3$/DMM ≤ 1, $NH_3$ behavior remains largely unchanged, with DMM chemistry clearly prevailing in the mixture.

NO (Fig. 4C) shows a clear difference for $NH_3$/DMM = 10, compared to the rest of ratios. This is attributed to the shift of all reactions toward higher temperatures and to the reduced relevance of NO consumption by $NH_2$ radicals, $NH_2 + NO \rightleftharpoons N_2 + H_2O$ (r23), which occurs because of a lower concentration of $NH_2$ radicals. In all cases, NO production reactions are equivalent to those discussed in the previous section. However, at high temperatures (T > 1200 K), differences are observed among the samples studied. For high DMM concentrations ($NH_3$/DMM = 0.5), NO production shifts to alternative pathways, mainly $HNO + H \rightleftharpoons NO + H_2$ (r67) and $NO_2 + H \rightleftharpoons NO + OH$ (r68). In contrast, as DMM decreases, $C_2H_4 + HNO \rightleftharpoons C_2H_5 + NO$ (-r20) becomes the main pathway for NO formation. In both cases, HNO acts as the key promoter of NO, primarily originating from $NH + O_2 \rightleftharpoons HNO + O$ (r69) and $NH_2 + O_2 \rightleftharpoons HNO + H$ (r70). These reactions do not directly involve carbon compounds. It should be noted that increasing DMM (as when $NH_3$/DMM = 0.5), NO concentrations remain similar to those presented for $NH_3$/DMM ≤ 1, despite that the initial concentration of $NH_3$ is half.

Another compound affected by the $NH_3$/DMM mixture ratio is $H_2$ (Fig. 4D). At the onset of the reaction, $H_2$ is formed via hydrogen

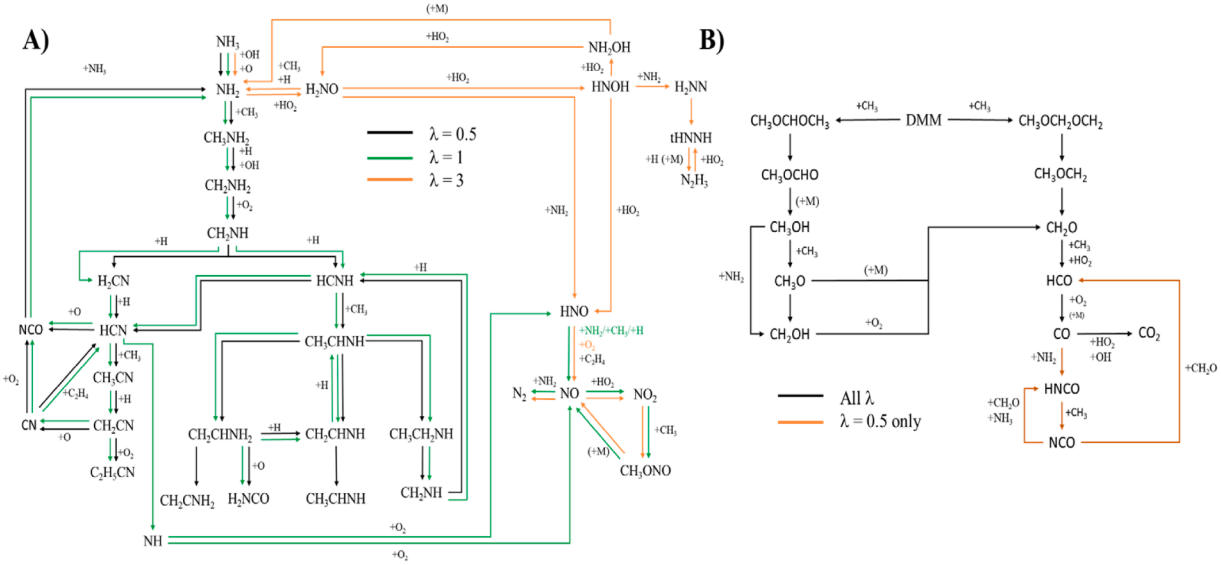


**Fig. 5.** Reaction pathways for A) $NH_3$ and B) DMM at $NH_3$/DMM=1 as a function of λ.

abstraction from DMM through interactions with H radicals, DMM + H ⇌ $CH_3OCHOCH_3$ + $H_2$ (r34) and DMM + H ⇌ $CH_3OCH_2OCH_2$ + $H_2$ (r35), for $NH_3$/DMM ≤ 1. Alternatively, the main $H_2$ production pathway involves reactions with formaldehyde, $CH_2O$ + H ⇌ HCO + $H_2$ (r67). $H_2$ consumption is not significantly affected by changes in the fuel proportions.

Several carbon-containing compounds exhibit variations with varying $NH_3$/DMM, i.e. DMM (Fig. 4B), $C_2H_6$ (Fig. 4E), and $C_2H_4$ (Fig. 4F). In general, the differences observed in the species profiles arise from changes in the initial DMM concentration rather than from modifications in its kinetic behavior.

Although it is generally observed that a higher proportion of DMM in the mixture leads to a shift of its oxidation temperatures, this trend is not observed for pure DMM. This behavior is attributed to the lower concentration of OH radicals, with hydrogen abstraction being predominantly initiated by $CH_3$ radicals. However, DMM is present at sufficient concentration in the fuel mixture ($NH_3$/DMM ≤ 1), it is primarily consumed via hydrogen abstraction by radicals such as OH and H. However, when the initial DMM concentration is reduced, the contribution of these radicals decreases drastically, leaving interactions with $CH_3$ as the dominant pathways, DMM + $CH_3$ ⇌ $CH_3OCH_2OCH_2$ + $CH_4$ (r16) and DMM + $CH_3$ ⇌ $CH_3OCHOCH_3$ + $CH_4$ (r18). This behavior is reflected in the DMM species profile (Fig. 4B). These reactions are also predominant in pure DMM hydrogen abstraction, partly due to the low production of OH radicals. Experimentally, however, this shift is not observed, suggesting that additional DMM decomposition reactions at low concentrations are not accounted for in the mechanism. When higher amounts of DMM are added ($NH_3$/DMM = 0.5), its consumption is observed only at lower temperatures in the final region of the reaction zone (T = 1025 K).

Regarding $C_2H_6$ and $C_2H_4$, it can be observed that their production shifts to higher temperatures when the initial DMM concentration is reduced ($NH_3$/DMM = 10). However, the main production reactions remain the same as those described in the previous section. This pattern is similar to DMM consumption. At these temperatures ($NH_3$/DMM = 10), fewer $CH_3$ radicals are available, making interactions with H radicals, $C_2H_6$ + H ⇌ $C_2H_5$ + $H_2$ (r52), and OH radicals, $C_2H_6$ + OH ⇌ $C_2H_5$ + $H_2O$ (r53), more significant. At $NH_3$/DMM = 10, $C_2H_4$ is mainly consumed by $C_2H_4$ + $NH_2$ ⇌ $C_2H_3$ + $NH_3$ (r57), which coincides with what happens under pyrolysis conditions. In the oxidation of pure DMM, the formation and consumption reactions of both species behave similarly to those observed for $NH_3$/DMM mixture ratios ≤ 1.

### 4.3. Reaction pathways

Fig. 5A illustrates the $NH_3$ reaction pathways under the investigated conditions: fuel-rich (black), stoichiometric (green), and fuel-lean (orange). The initial consumption of $NH_3$ proceeds through the same pathways in all cases, $NH_3$ + OH ⇌ $NH_2$ + $H_2O$ (r8) and $NH_3$ + O ⇌ $NH_2$ + OH (r9), leading to the formation of $NH_2$ radicals. Additionally, new reaction pathways are active when λ > 1. Nevertheless, at low initial $O_2$ concentration (λ ≤ 1), and under conditions of high $CH_3$ radical concentration, the $NH_2$ radical tends to react with $CH_3$, $CH_3$ + $NH_2$ ⇌ $CH_3NH_2$ (r31). Subsequently, $CH_3NH_2$ undergoes hydrogen abstraction via interactions with radicals such as H and OH. The $CH_2NH$ intermediate can then react with H radicals via two alternative pathways, forming either $H_2CN$, $CH_2NH$ + H ⇌ $H_2CN$ + $H_2$ (r72), or HCNH, $CH_2NH$ + H ⇌ HCNH + $H_2$ (r73). This reaction pathway is denoted as R1.

**R1.** $NH_3$→$CH_3NH_2$→$CH_2NH_2$→$CH_2NH$→$H_2CN$/HCNH

The HCNH formed can follow two distinct reaction pathways: the production of HCN, HCNH ⇌ HCN + H (r74), and the formation of $CH_3CHNH$, HCNH + $CH_3$ ⇌ $CH_3CHNH$ (r75). From $CH_3CHNH$, successive decomposition reactions take place, with only limited interaction with radicals such as O, $CH_2CHNH_2$ + O ⇌ $H_2NCO$ + $CH_3$ (r76). Species derived from $CH_3CHNH$ tend to regenerate $NH_2$ radicals under fuel-rich conditions (λ ≤ 1), designated as pathway R2.

**R2.** HCNH→$CH_3CHNH$→$CH_2CHNH_2$/$CH_2CHNH$/ $CH_2NH_2NH$

In addition to reaction (r71), HCN is also formed via $H_2CN$, $H_2CN$ + $H$ ⇌ HCN + $H_2$ (r77). Following the reaction pathway denoted as R3, it is evident that the $NH_2$ radical is recycled to $NH_3$.

**R3.**$CH_2NH$→HCN→$CH_3CN$→$CH_2CN$→CN→NCO→$NH_2$

However, when HCN is present under higher $O_2$ concentrations (λ = 1), it reacts to form NH, HCN + O ⇌ NH + CO (r78). From this NH, subsequent reactions lead to the formation of NO, NH + $O_2$ ⇌ NO + OH (r79), and HNO, NH + $O_2$ ⇌ HNO + O (r69), reaction pathway R4.

**R4.** HCN→NH→HNO

When HNO and NO are formed, their conversion leads to the formation of $N_2$, as has been extensively described (R5-R6) [e.g. 9,27]. These pathways occur whenever there is sufficient $O_2$ in the combustion mixture (λ ≥ 1).

**R5.** HNO→NO→$N_2$

**R6.** NO→$NO_2$→$CH_3ONO$→NO

Under fuel-lean conditions, a reaction pathway distinct from those previously described has been identified, leading to the formation of HNO. Initially, the $NH_2$ radical reacts with $HO_2$ radicals to form $H_2NO$, $NH_2$ + $HO_2$ ⇌ $H_2NO$ + OH (r3).

**R7.** $NH_3$→$NH_2$→$H_2NO$

Although $H_2NO$ provides a secondary pathway for the formation of $N_2H_3$, HNO is primarily produced via $H_2NO$ + $NH_2$ ⇌ HNO + $NH_3$ (r80). Subsequently, HNO participates in reactions as described in pathways R5 and R6. $N_2$ formation occurs exclusively through $NH_2$ + NO ⇌ $N_2$ + $H_2O$ (r23) when the fuel concentrations are equal ($NH_3$/DMM = 1).

The reaction pathways of $NH_3$ under stoichiometric conditions were compared for various $NH_3$/DMM mixture ratios, evaluated at temperatures corresponding to 10% $NH_3$ consumption. As the DMM concentration increases ($NH_3$/DMM = 0.5), the reaction pathway appears to be equivalent to that previously presented in Fig. 5A.

However, at a substantially higher $NH_3$ concentration ($NH_3$/DMM = 10), a series of changes in the reaction behavior are observed. No differences are apparent up to the formation of $CH_3CHNH$. Beyond this point, it has been observed that this species does not produce a wide range of decomposition products, but rather follows a linear reaction pathway, as described in R8.

**R8.** HCNH→$CH_3CHH$→$CH_3CH_2NH$→$CH_2NH$→$H_2CN$

Another significant change is the emergence of an additional pathway for NO consumption, $NH_2$ + NO ⇌ NNH + OH (r24), which becomes relevant due to the increased concentration of $NH_2$ radicals. This results in pathway R9.

**R9.** NO→NNH→$N_2$

Regarding DMM, its initial consumption occurs primarily through hydrogen abstraction by $CH_3$ radicals. Consequently, the first intermediate compounds of DMM are formed via the reactions DMM + $CH_3$ ⇌ $CH_3OCH_2OCH_2$ + $CH_4$ (r16) and DMM + $CH_3$ ⇌ $CH_3OCHOCH_3$ + $CH_4$ (r18). Once $CH_3OCHOCH_3$ is formed, it decomposes into $CH_3OCHO$ and $CH_3$. As mentioned above, methyl formate produces only $CH_3OH$ and CO, via $CH_3OCHO$ (+M) ⇌ $CH_3OH$ + CO (+M) (r45). This entire reaction pathway is represented in R10.

**R10.** DMM→$CH_3OCHOCH_3$→$CH_3OCHO$→$CH_3OH$

Starting from methanol, formaldehyde ($CH_2O$) is eventually formed

**Novelty and significance statement**

This paper presents a detailed species profile study of the conversion of $NH_3$/DMM fuel mixture at atmospheric pressure in a flow reactor installation. To the authors' knowledge, no previous studies have reported such detailed experimental speciation data in a flow reactor. The experimental results reported here contribute to the currently limited database for $NH_3$/DMM mixtures, while the kinetic model presented represents an initial step towards the development of a more robust kinetic mechanism for nitrogen-carbon fuel systems.

through three different pathways. The first two pathways involve the formation of $CH_2O$ without the participation of $NH_2$ radicals, relying exclusively on interactions with carbon-containing compounds. Methanol reacts with $CH_3$ radicals, $CH_3OH + CH_3 \rightleftharpoons CH_3O + CH_4$ (r46). $CH_3O$ can then directly produce $CH_2O$ via interaction with a third body, $CH_3O (+M) \rightleftharpoons CH_2O + H (+M)$ (r81). Alternatively, a hydrogen radical may migrate within $CH_3O$, forming $CH_2OH$, $CH_3O \rightleftharpoons CH_2OH$ (r82). This $CH_2OH$ radical can subsequently generate $CH_2O$ through its oxidation with $O_2$, $CH_2OH + O_2 \rightleftharpoons CH_2O + HO_2$ (r83). These pathways are represented in R11 and R12.

**R11.** $CH_3OH \rightarrow CH_3O \rightarrow CH_2O$

**R12.** $CH_3O \rightarrow CH_2OH \rightarrow CH_2O$

Another important pathway for $CH_3OH$ consumption occurs through its interaction with $NH_2$ radicals, $CH_3OH + NH_2 \rightleftharpoons CH_2OH + NH_3$ (r84). This reaction has previously been identified as significant by Wang et al. [41].

**R13.** $CH_3OH \rightarrow CH_2OH \rightarrow CH_2O$

$CH_3OCH_2OCH_2$ also produces $CH_2O$ as its main intermediate compound. Initially, $CH_3OCH_2OCH_2$ decomposes into $CH_3OCH_2$ via the reaction $CH_3OCH_2OCH_2 \rightleftharpoons CH_3OCH_2 + CH_2O$ (r85). As a result of this reaction, $CH_2O$ is already being formed. $CH_3OCH_2$ then continues to decompose, generating additional $CH_2O$. This reaction pathway is represented in R14.

**R14.** $CH_3OCH_2OCH_2 \rightarrow CH_3OCH_2 \rightarrow CH_2O$

Starting from $CH_2O$, $CH_2O$ reacts with $CH_3$ radicals to produce HCO, $CH_2O + CH_3 \rightleftharpoons HCO + CH_4$ (r86). Under fuel-lean conditions, interactions with $HO_2$ radicals become more significant, $CH_2O + HO_2 \rightleftharpoons HCO + H_2O_2$ (r14). HCO preferentially decomposes to CO via HCO (+M) $\rightleftharpoons$ H + CO (+M) (r63). Finally, CO is oxidised to $CO_2$ through the reactions $CO + OH \rightleftharpoons CO_2 + H$ (r65) and $CO + HO_2 \rightleftharpoons CO_2 + OH$ (r66).

**R15.** $CH_2O \rightarrow HCO \rightarrow CO \rightarrow CO_2$

At $\lambda \leq 1$, $CO_2$ formation from CO is limited; and the interaction of CO with $NH_2$ radicals, $CO + NH_2 \rightleftharpoons HNCO + H$ (r87), produces HNCO. Simultaneously, HNCO decomposes into NCO via $HNCO + CH_3 \rightleftharpoons NCO + CH_4$ (r88).

**R16.** $CO \rightarrow HNCO \rightarrow NCO$

The reaction pathways of DMM under stoichiometric conditions were compared across various $NH_3$/DMM mixture ratios. The analysis revealed no significant differences in the reaction pathways predicted by the mechanism. So, that indicates that the reaction pathways of DMM are roughly independent of the initial $NH_3$ concentration in the fuel mixture.

## 5. Conclusions

The present study provides a comprehensive investigation of the influence of the $NH_3$/DMM ratio on the conversion of reactants and formation of a variety of products in a flow reactor at atmospheric pressure. Experiments were conducted over a broad range of $\lambda$ (0–3.12) and $NH_3$/DMM ratios (0.48–10.86), across temperatures of 875–1425 K. Detailed species profiles were obtained, many of which have not been extensively characterized to date. Calculations with an updated detailed kinetic mechanism show good agreement with the overall trends observed for the key species.

Analysis of the effect of $\lambda$ offered valuable insights into how the initial $O_2$ concentration influences the fuel mixture conversion. $NH_3$ was found to be highly sensitive to variations in $O_2$, whereas DMM displayed minimal changes, with no appreciable shift (≈50 K) in its reaction temperature.

The OH radical is fundamental for $NH_3$ consumption in the mixture. Many of the main DMM consumption reactions favour $NH_3$ oxidation, as they do not compete for OH and O radicals. The main consumption of DMM occurs through the abstraction of hydrogen from the central carbon, by interaction with $CH_3$ radicals.

Furthermore, DMM has been found to exert a significant influence on the $NH_3$ behavior, particularly for $NH_3$/DMM $\leq 1$. This effect diminishes at higher initial $O_2$ concentrations ($\lambda > 1$), as the reaction proceeds along pathways involving almost exclusively $NH_3$ and derivatives. The formation of the most important intermediate compounds of $NH_3$ net combustion ($H_2NO$ and HNO) takes place, as well as the characteristic emissions (NO and $N_2$).

## Supplementary material

Supplementary material associated with this article can be found in the online version.

## CRediT authorship contribution statement

**Adrián Ruiz-Gutiérrez:** Writing – original draft, Software, Formal analysis, Data curation, Conceptualization. **Daniel Mazano-Peña:** Data curation. **María U. Alzueta:** Writing – review & editing, Validation, Supervision, Project administration, Conceptualization.

## Declaration of competing interest

The authors declare that they have no known competing financial interests or personal relationships that could have appeared to influence the work reported in this paper.

## Acknowledgments

The authors express their gratitude to grant PID2021-12432OB-I00, TED2021-129557B-I00 and PID2025-155489OB-I00, funded by MCIN/AEI/10.13039/501100011033, "ERDF A way of making Europe" and COST Action CA22151, by the "European Union" and to Aragón Government (Ref. T22_23R) and pre-doctoral grant awarded to Mr. Ruiz-Gutiérrez, PRE2022-104181 grant funded by MICIN.

## Supplementary materials

Supplementary material associated with this article can be found, in the online version, at doi:10.1016/j.combustflame.2026.114966.

## References


[1] Greenhouse gas emissions by country and sector (infographic) – Topics – European Parliament,https://www.europarl.europa.eu/topics/en/article/20180301STO98928/greenhouse-gas-emissions-by-country-and-sector-infographic (accessed December 9, 2025).

[2] How is EU electricity produced and sold? – Consilium, https://www.consilium.europa.eu/en/infographics/how-is-eu-electricity-produced-and-sold/(accessed December 9, 2025).

[3] Climate report shows the largest annual drop in EU greenhouse gas emissions for decades – European Commission, https://commission.europa.eu/news/climate-report-shows-largest-annual-drop-eu-greenhouse-gas-emissions-decades-2024-11-05_en (accessed December 9, 2025).

[4] S. Zhu, Q. Xu, R. Tang, J. Gao, Z. Wang, J. Pan, et al., A comparative study of oxidation of pure ammonia and ammonia/dimethyl ether mixtures in a jetstirred reactor using SVUV-PIMS, Combust. Flame 250 (2023) 112643, https://doi.org/10.1016/j.combustflame.2023.112643.

[5] N. Campion, H. Nami, P.R. Swisher, P. Vang Hendriksen, M. Münster, Technoeconomic assessment of green ammonia production with different wind and solar potentials, Renew. Sust. Energy Rev. 173 (2023) 113057, https://doi.org/10.1016/j.rser.2022.113057.

[6] Q. Guo, J. Liu, L. Zhang, X. Feng, H. Wang, Explosion limits of binary mixtures of ammonia and additives (hydrogen, natural gas, and diethyl ether), Fuel 381 (2025) 133519, https://doi.org/10.1016/j.fuel.2024.133519.

[7] M. Li, X. He, H. Hashemi, P. Glarborg, V.M. Lowe, P. Marshall, R. Fernandes, B. Shu, An experimental and modelling study on autoignition kinetics of ammonia/methanol mixtures at intermediate temperature and high pressure, Combust. Flame 242 (2022) 112160, https://doi.org/10.1016/j.combustflame.2022.112160.

[8] G. Issayev, B.R. Giri, A.M. Elbaz, K.P. Shrestha, F. . Mauss, W.L. Roberts, A. Farooq, Ignition delay time and laminar flame speed measurements of ammonia blended with dimethyl ether: a promising lowcarbon fuel blend, Renew. Energy 181 (2022) 1353–1370, https://doi.org/10.1016/j.renene.2021.09.117.

[9] A. Ruiz-Gutiérrez, P. Rebollo, M.U. Alzueta, Combustion of $NH_3$/DME and $NH_3$/DME/NO mixtures, Fuel 381 (2025) 133253, https://doi.org/10.1016/j.fuel.2024.133253.

[10] A. Ruiz-Gutiérrez, I. De Diego, M.U. Alzueta, Use of methanol as a promoter for ammonia combustion, BioMass BioEnergy 193 (2025) 107572, https://doi.org/10.1016/j.biombioe.2024.107572.

[11] Z. Wang, X. Han, Y. He, R. Zhu, Y. Zhu, Z. Zhou, et al., Experimental and kinetic study on the laminar burning velocities of $NH_3$ mixing with $CH_3OH$ and $C_2H_5OH$ in premixed flames, Combust. Flame 229 (2021) 111392, https://doi.org/10.1016/j.combustflame.2021.02.038.

[12] X. Shi, W. Li, J. Zhang, Q. Fang, Y. Zhang, Z. . Xi, et al., Exploration of $NH_3$ and $NH_3$/DME laminar flame propagation in $O_2/CO_2$ atmosphere: insights into $NH_3/CO_2$ interactions, Combust. Flame 260 (2024) 113245, https://doi.org/10.1016/j.combustflame.2023.113245.

[13] A. Omari, B. Heuser, S. Pischinger, Potential of oxymethylenetherdiesel blends for ultralow emission engines, Fuel 209 (2017) 232–237, https://doi.org/10.1016/j.fuel.2017.07.107.

[14] F. Viteri, K. Alexandrino, Á. Millera, R.. Bilbao, M.U.. Alzueta, Polycyclic aromatic hydrocarbons formed during the pyrolysis of dimethoxymethane (DMM): comparison with other oxygenated additives, Fuel 383 (2025) 133750, https://doi.org/10.1016/j.fuel.2024.133750.

[15] Y. Ren, Z. Huang, H. Miao, Y. Di, D. Jiang, K. Zeng, et al., Combustion and emissions of a DI diesel engine fuelled with dieseloxygenate blends, Fuel 87 (2008) 2691–2697, https://doi.org/10.1016/j.fuel.2008.02.017.

[16] L. Marrodán, Á. Millera, R. Bilbao, M.U. Alzueta, Experimental and modelling evaluation of dimethoxymethane as an additive for highpressure acetylene oxidation, J. Phys. Chem. A 126 (2022) 6253–6263, https://doi.org/10.1021/acs.jpca.2c03130.

[17] W.X. Wang, X.J. Gao, P. Xiong, J.F. Zhang, F.E. Song, Q. Zhang, et al., Lowtemperature oxidation of methanol to dimethoxymethane over Mo–Sn catalyst, J. Fuel Chem. Technol. 49 (2021) 1487–1494, https://doi.org/10.1016/S1872-5813(21)60094-4.

[18] M. Pan, W. Qian, Y. Wang, C. Wu, H. Huang, Effect of dimethoxymethane (DMM) additive on combustion and emission characteristics under different working conditions in CI engines, Fuel 284 (2021) 119304, https://doi.org/10.1016/j.fuel.2020.119304.

[19] A. Albinet, E. LeozGarziandia, H. Budzinski, E. Villenave, J.L. Jaffrezo, Nitrated and oxygenated derivatives of polycyclic aromatic hydrocarbons in the ambient air of two French alpine valleys. Part 1: concentrations, sources and gas/particle partitioning, Atmos. Environ. 42 (2008) 43–54, https://doi.org/10.1016/j.atmosenv.2007.10.009.

[20] A.M. Elbaz, B.R. Giri, A. Issayev, K.P. Shrestha, F. Mauss, A. Farooq, et al., Experimental and kinetic modelling study of laminar flame speed of dimethoxymethane and ammonia blends, Energy Fuels. 34 (2020) 14726–14740, https://doi.org/10.1021/acs.energyfuels.0c02269.

[21] L. Dai, Y. Yuan, Q. Lin, W. Li, C. Zou, J. Liu, et al., Shocktube and modelling study on the ignition delay times of ammonia/dimethoxymethane at high temperature, Combust. Flame 256 (2023) 112967, https://doi.org/10.1016/j.combustflame.2023.112967.

[22] S. Wang, A.M. Elbaz, Z. Wang, W.L. Roberts, The laminar and turbulent flame speed of methanol/ammonia/air, ethylacetate/ammonia/air, and dimethoxymethane/ammonia/air under atmospheric and elevated pressures, Combust. Flame 277 (2025) 114187, https://doi.org/10.1016/j.combustflame.2025.114187.

[23] Y. Yin, Q. Cheng, Y. Qiao, Q. Dong, X. Meng, Towards clean and renewable energy: construction of the premixed ammonia/dimethoxymethane chemical reaction mechanism and numerical simulation analysis, Energy 319 (2025) 134827, https://doi.org/10.1016/j.energy.2025.134827.

[24] M.U. Alzueta, J.M. Hernández, M. Finestra, Methanol oxidation and its interaction with nitric oxide, Energy Fuels 15 (2001) 724–729, https://doi.org/10.1021/ef0002602.

[25] L. Marrodán, F. Monge, Á. Millera, R. Bilbao, M.U. Alzueta, Dimethoxymethane oxidation in a flow reactor, Combust. Sci. Technol. 188 (2016) 719–729, https://doi.org/10.1080/00102202.2016.1138826.

[26] A. Ruiz-Gutiérrez, A. Bello-Gallego, M.U. Alzueta, Flow reactor study of $NH_3$/DEE oxidation chemistry, Energy Fuels. 39 (2025) 16407–16421, https://doi.org/10.1021/acs.energyfuels.5c01874.

[27] P. Glarborg, J.A. . Miller, B. Ruscic, S.J. Klippenstein, Modelling nitrogen chemistry in combustion, Prog. Energy Combust. Sci. 67 (2018) 31–68, https://doi.org/10.1016/j.pecs.2018.01.002.

[28] M.U. Alzueta, M. Abián, I. Elvira, V.D.. Mercader, L. Sieso, Unraveling the NOreduction mechanisms occurring during the combustion of $NH_3/CH_4$ mixtures, Combust. Flame 257 (2022) 112531, https://doi.org/10.1016/j.combustflame.2022.112531.

[29] J. Jian, H. Hashemi, H. Wu, P. Glarborg, A.W. . Jasper, S.J. . Klippenstein, An experimental, theoretical and kinetic modelling study of postflame oxidation of ammonia, Combust. Flame 261 (2024) 113325, https://doi.org/10.1016/j.combustflame.2024.113325.

[30] C.P. Morell, C.K. Juhl, A. Chanpirak, H. Hashemi, H. Wu, P. Glarborg, Reexamination of the HNCO oxidation chemistry, Fuel 385 (2025) 134090, https://doi.org/10.1016/j.fuel.2024.134090.

[31] L. Marrodán, A. Millera, R. Bilbao, M.U. Alzueta, An experimental and modelling study of acetylenedimethyl ether mixtures oxidation at high pressure, Fuel 327 (2022) 125143, https://doi.org/10.1016/j.fuel.2022.125143.

[32] L.S. Tran, J. Pieper, H.H. Carstensen, H. Zhao, I. . Graf, Y. Ju, et al., Experimental and kinetic modelling study of diethyl ether flames, Proc. Combust. Inst. 36 (2017) 1165–1173, https://doi.org/10.1016/j.proci.2016.06.087.

[33] L. Marrodán, Á. Millera, R. Bilbao, M.U. Alzueta, Experimental and modelling evaluation of dimethoxymethane as an additive for highpressure acetylene oxidation, J. Phys. Chem. A 126 (2022) 6253–6263, https://doi.org/10.1021/acs.jpca.2c03130.

[34] P. García-Ruiz, M. Abián, M.U. Alzueta, Oxidation of diethyl ether/ammonia mixtures in a flow reactor at different pressures, Fuel 413 (2026) 138129, https://doi.org/10.1016/j.fuel.2025.138129.

[35] A. Lucassen, K. Zhang, J. Warkentin, K. Moshammer, P. Glarborg, P. Marshall, et al., Fuelnitrogen conversion in the combustion of small amines using dimethylamine and ethylamine as biomassrelated model fuels, Combust. Flame 159 (2012) 2254–2279, https://doi.org/10.1016/j.combustflame.2012.02.024.

[36] K.P. Shrestha, B.R. Giri, A.M. Elbaz, G. Issayev, W.L. Roberts, L. Seidel, et al., A detailed chemical insight into the kinetics of diethyl ether enhancing ammonia combustion and the importance of $NO_x$ recycling mechanism, Fuel Commun. 10 (2022) 100051, https://doi.org/10.1016/j.jfueco.2022.100051.

[37] W. Sun, T. Tao, M. Lailliau, N. Hansen, B. Yang, P. Dagaut, Exploration of the oxidation chemistry of dimethoxymethane: jetstirred reactor experiments and kinetic modelling, Combust. Flame 193 (2018) 491–501, https://doi.org/10.1016/j.combustflame.2018.04.008.

[38] Y. Yin, Q. Cheng, Y. Qiao, Q. Dong, X. Meng, Towards clean and renewable energy: construction of the premixed ammonia/dimethoxymethane chemical reaction mechanism and numerical simulation analysis, Energy 319 (2025), https://doi.org/10.1016/j.energy.2025.134827.

[39] Y. Zhang, Q. Wang, L. Dai, M. Zhang, C. Yu, Numerical study on the combustion properties of ammonia/DME and ammonia/DMM mixtures, Energies 16 (2023) 6929, https://doi.org/10.3390/en16196929.

[40] M.U. Alzueta, T. Pérez, L. Marrodán, Oxidation of methylamine ($CH_3NH_2$)/$CH_4$/NO mixtures in an atmospheric-pressure flow reactors, Proc. Combust. Inst. 40 (2024) 105456, https://doi.org/10.1016/j.proci.2024.105456.

[41] Z. Wang, B. Mei, N. Liu, A. Thawko, X. Mao, H. Zhao, et al., Highpressure ammonia/methanol oxidation up to 100 atm, Proc. Combust. Inst. 40 (2024) 105489, https://doi.org/10.1016/j.proci.2024.105489.